Pergamon

Int. J. Heat Mass Transfer. Vol. 39, No. 1, pp. 203–210, 1996

0017-9310/96 $9.50+0.00

0017–9310(95)00107–7

Free convection heat transfer of non-Newtonian fluids over axisymmetric and two-dimensional bodies of arbitrary shape embedded in a fluid-saturated porous medium

YUE-TZU YANG and SAE-JAN WANG

Department of Mechanical Engineering, National Cheng Kung University, Tainan, Taiwan 70101, Republic of China

(*Received* 10 *August* 1994)

Abstract—The problem of natural convection of a non-Newtonian power-law fluid with or without yield stress about a two-dimensional or axisymmetric body of arbitrary shape in a fluid-saturated porous medium is analyzed on the basis of boundary layer approximation. For a high modified Rayleigh number, similarity solutions are obtained by using the fourth-order Runge–Kutta scheme and shooting method for two-dimensional bodies without yield stress and a cone with yield stress. The effects of the surface heat transfer rate $q_w(x)$, the local Nusselt number Nu_x, the overall heat transfer rate Q^* and the power indices n of fluids with the yield stresses on the free convection heat transfer characteristics are discussed. It is found that the results depend strongly on the high values of the yield stress parameter Ω/a at the boundary.

INTRODUCTION

Owing to practical engineering interests, the predictions of natural convection heat transfer rate on bodies embedded in a fluid-saturated porous medium have been extensively studied and reported for Newtonian fluids, for example in refs. [1–4]. However, relatively little attention has been given to the natural convection of a non-Newtonian fluid in a porous medium [5–14].

The present study applies the Al-Fariss modified Darcy's law and the Herschel–Bulkley model [8] to the fundamental flow and energy equations in a porous medium, for non-Newtonian fluids with viscosity depending strongly on shear rate as

$$\tau = H\dot{\gamma}^n + \tau_0 \text{ for } \tau > \tau_0$$

where n, H and τ_0 are rheological parameters to be determined from tests and $\dot{\gamma}$ is the shear rate. For values of n less than unity, the behavior is pseudo-plastic with yield stress, whereas for n greater than unity the behavior is dilatant with yield stress. For $n = 1.0$ and $\tau_0 = 0$, it reduces to Newton's law of viscosity. Pascal [12, 13] has analyzed theoretically the application of Darcy's law to shear thinning fluids with the yield value and obtained solutions for wall flow test analyses.

In this paper, it is assumed that the modified Darcy's law with the boundary layer approximation can be applied correctly. This implies that the present solutions are effective at a high modified Rayleigh number. Under these simplifications, the similarity solutions can be obtained from the governing equations by using the fourth-order Runge–Kutta method and the shooting method. The main objective of this study was to predict the flow behavior and the surface heat transfer rate of bodies.

ANALYSIS

To describe the rheological behavior effects of non-Newtonian fluids flowing through a porous medium, a modified Darcy's law is required. In accordance with a previous report [8], the model of laminar flow of a non-Newtonian power-law fluid with yield stress through a porous medium is used here. According to the rheological effect of a non-Newtonian fluid of Bingham type, the modified Darcy's law can be written as:

$$u = \left[\frac{k}{\mu_{ef}}\left(-\frac{\partial P}{\partial x} - \alpha_0\right)\right]^{1/n} \quad \left|\frac{\partial P}{\partial x}\right| > \alpha_0 \quad u \neq 0$$

$$\left|\frac{\partial P}{\partial x}\right| \leqslant \alpha_0 \quad u = 0 \tag{1}$$

with k and μ_{ef} being expressed in terms of the rheological parameters n, H, D_p, ε and C' as:

$$\mu_{ef} = \frac{H}{4}\left(3 + \frac{1}{n}\right)^n (8C'\varepsilon k)^{(1-n)/2} \tag{2}$$

and

NOMENCLATURE

C'	tortuosity factor
D_p	particle size
f	similarity stream function
g	gravity
H	consistency index
k	permeability
k_{ef}	effective thermal conductivity
l	reference length
n	power index of non-Newtonian fluid
Nu_x	local Nusselt number, equation (31)
P	pressure
Ra_n	modified Rayleigh number, equation (13)
T	temperature
u, v	Darcian velocity components
x, y	coordinates.

Greek symbols

α_0	Threshold gradient
α_{ef}	effective thermal diffusivity
β	coefficient of thermal expansion
$\dot{\gamma}$	shear rate
δ_m	momentum boundary layer thickness
δ_t	thermal boundary layer thickness
ε	porosity of porous medium
φ	similarity variable
η	similarity variable
θ	dimensionless temperature
λ	constant
μ_{ef}	effective viscosity
ρ	density of fluid
τ	shear stress
τ_0	yield stress
ϕ	angle
ψ	dimensionless stream function
Ω	dimensionless yield stress.

Subscripts

w	wall property
x	local property
∞	ambient property of porous medium.

Superscript

*	dimensionless property.

$$k = D_p^2\varepsilon^3/[72C'(1-\varepsilon)^2]. \quad (3)$$

The threshold gradient α_0 in equation (1) is related to the yield stress τ_0:

$$\alpha_0 = \frac{\lambda\tau_0}{\sqrt{k}} \quad (4)$$

where λ is a non-dimensional constant to be determined experimentally, k is permeability, C' is the tortuosity factor, ε is porosity and D_p is particle size. Bird [15] used an average value of $C' = 25/12$.

The physical model and coordinate system are shown in Fig. 1. Coordinate x is measured around the body surface from the lowest point (0,0) and y is set perpendicular to the body surface at any point. The governing equations to be used for conservation of mass, momentum and energy are in accordance with the following assumptions: (i) the temperature of the fluid everywhere is below the boiling point and over the condensating point so that no two-phase zone exists; (ii) the convective fluid and the porous medium are in local thermodynamic equilibrium everywhere; (iii) the thermophysical properties of the fluid and the porous medium remain constant except in the buoyancy term itself; (iv) the free convection flow is in uniform steady state, laminar flow; (v) the fluid is a Herschel–Bulkley model fluid; and (vi) the Boussinesq approximation can be employed. Thus, the governing equations are given as:

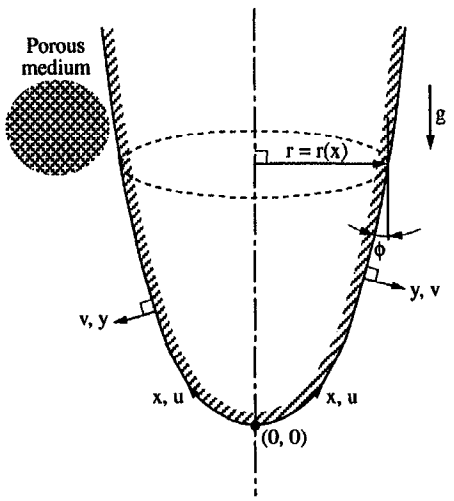

Fig. 1. Physical model and coordinate system.

$$\frac{\partial r^m u}{\partial x} + \frac{\partial r^m v}{\partial y} = 0 \quad (5)$$

$$u^n = \frac{k\rho_\infty g\beta}{\mu_{ef}}\left([T-T_\infty]\cos\phi - \frac{\alpha_0}{\rho_\infty g\beta}\right)$$

$$\text{if } |(T-T_\infty)\cos\phi| > \frac{\alpha_0}{\rho_\infty g\beta}$$

$$u = 0 \quad \text{if } |(T-T_\infty)\cos\phi| \leqslant \frac{\alpha_0}{\rho_\infty g\beta} \quad (6)$$

$$u\frac{\partial T}{\partial x} + v\frac{\partial T}{\partial y} = \alpha_{ef}\left(\frac{\partial^2 T}{\partial x^2} + \frac{\partial^2 T}{\partial y^2}\right) \quad (7)$$

where $\cos\phi = \sqrt{[1-(\mathrm{d}r/\mathrm{d}x)^2]}$, $m = 0$ for two-dimen-

sional bodies and $m = 1$ for axisymmetric bodies, u and v are the Darcian velocity components in the x and y directions, T is the local temperature, α_{ef} is the effective thermal diffusivity of the porous medium and β is the coefficient of thermal expansion. The appropriate boundary conditions are

$$y = 0 \quad T = T_w \quad v = 0 \tag{8}$$

$$y \to \infty \quad T = T_\infty \quad u = 0 \tag{9}$$

where T_w indicates the wall temperature and T_∞ refers to the ambient temperature.

Under the boundary layer approximations, the dimensionless equations can be written as:

$$\frac{\partial (r^*)^m u^*}{\partial x^*} + \frac{\partial (r^*)^m v^*}{\partial y^*} = 0 \tag{10}$$

$$u^* = (\theta S - \Omega)^{1/n} \quad \text{if } |\theta S| > \Omega \tag{11}$$

$$u^* = 0 \quad \text{if } |\theta S| \leqslant \Omega$$

$$u^* \frac{\partial \theta}{\partial x^*} + v^* \frac{\partial \theta}{\partial y^*} = \frac{\partial^2 \theta}{\partial y^{*2}} \tag{12}$$

with the following dimensionless variables introduced:

$$x^* = x/l \quad y^* = y/l \quad \theta = (T - T_\infty)/(T_w - T_\infty)$$

$$S = \cos\phi \quad r^* = r/l$$

$$\Omega = \frac{\alpha_0}{\rho_\infty g \beta (T_w - T_\infty)} \quad Ra_n = \left(\frac{\rho_\infty g \beta (T_w - T_\infty)}{\mu_{ef}}\right)^{1/n} \frac{l}{\alpha_{ef}}$$

$$u^* = \frac{ul}{Ra_n \alpha_{ef}} \quad v^* = \frac{vl}{Ra_n^{1/2} \alpha_{ef}}. \tag{13}$$

Note that Ω is defined as the yield stress parameter and Ra_n is the modified Rayleigh number. Here l denotes the reference length and T_∞ indicates the ambient temperature. The dimensionless stream function φ can be defined to satisfy the continuity equation (10) automatically as:

$$u^* = \frac{1}{(r^*)^m} \frac{\partial \psi}{\partial y^*} \tag{14a}$$

$$v^* = \frac{-1}{(r^*)^m} \frac{\partial \psi}{\partial x^*}. \tag{14b}$$

The boundary conditions for solving equations (11), (12) and (14) are

$$y^* = 0 \quad \theta = 1 \quad v^* = 0 \tag{15}$$

$$y^* \to \infty \quad \theta = 0 \quad u^* = 0. \tag{16}$$

To obtain similarity solutions for equations (10)–(12) with boundary conditions, equations (15) and (16), the restrictive conditions of the following two cases are necessary.

Case 1

Consider the fluid as being a power-law fluid without yield stress. To transform equations (10)–(12) into a set of ordinary differential equations, we introduce the following general dimensionless transformations:

$$\varphi = \left(\int_0^{x^*} (r^*)^{2m} S^{1/n} \, d\xi\right)^{1/2} (\sqrt{2}) f(\eta) \tag{17}$$

$$\eta = y^* (r^*)^m S^{1/n} \Big/ \left[(\sqrt{2}) \left(\int_0^{x^*} (r^*)^{2m} S^{1/n} \, d\xi \right)^{1/2} \right]. \tag{18}$$

Thus, the dimensionless velocity components will be

$$u^* = S^{1/n} f'(\eta) \tag{19}$$

$$v^* = -\left(S^{1/n} f'(\eta) + f(\eta) \frac{(r^*)^m S^{1/n}}{(\sqrt{2}) \left[\int_0^{x^*} (r^*)^{2m} S^{1/n} \, d\xi \right]^{1/2}} \right). \tag{20}$$

Based on equations (13), (14), (16) and (17), we have

$$\theta'' + f\theta' = 0 \tag{21}$$

$$f' = \theta^{1/n} \tag{22}$$

$$f = 0 \quad \theta = 1 \quad \text{at } \eta = 0 \tag{23}$$

$$f' = 0 \quad \theta = 0 \quad \text{as } \eta \to \infty \tag{24}$$

where the primes indicate differentiation with respect to η.

Case 2

Consider a cone embedded in a porous medium saturated by a power-law fluid with yield stress. The following dimensionless variables are introduced:

$$\varphi = \left[\int_0^{x^*} (r^*)^{2m} \, d\xi \right]^{1/2} (a - \Omega)^{1/2n} (\sqrt{2}) f(\eta) \tag{25}$$

$$\eta = \frac{y^* (r^*)^m (a - \Omega)^{1/2n}}{(\sqrt{2}) \left[\int_0^{x^*} (r^*)^{2m} \, d\xi \right]^{1/2}} \tag{26}$$

where $a = \cos\phi$, $r^* = x^* \sqrt{(1 - a)^2}$.

With equations (13), (14) and appropriate boundary conditions, we have

$$\theta'' + f\theta' = 0 \tag{27}$$

$$\left(\theta - \frac{\Omega}{a}\right)^{1/n} = \left(1 - \frac{\Omega}{a}\right) f'^{1/n} \quad \text{if } |\theta| > \Omega/a \tag{27a}$$

$$f' = 0 \quad \text{if } |\theta| \leqslant \Omega/a \tag{27b}$$

whereas equations (23) and (24) still hold true.

According to Fourier's law of heat conduction, the local surface heat transfer rate $q_w(x)$ can be written as

$$q_w(x) = -k_{ef} \left. \frac{\partial T}{\partial y} \right|_{y=0}$$

$$= -\frac{Ra_n^{1/2} (T_w - T_\infty) k_{ef}}{l} \theta'(0) \frac{\partial \eta}{\partial y^*} \tag{28}$$

Table 1. Values of $[-\theta'(0)]$ and $f(\infty)$ in Case 1 for selected values of n

n:	3.0	2.0	1.8	1.4	1.2
$-\theta'(0)$	0.727492	0.6983038	0.6892931	0.6652817	0.6487795
$f(\infty)$	1.727492	1.698303	1.6021120	1.386557	1.2688990
n:	1.0	0.8	0.6	0.4	0.2
$-\theta'(0)$	0.62756	0.599215	0.5593105	0.4985619	0.3918385
$f(\infty)$	1.142639	1.005741	0.8542631	0.680778	0.4665254

	Present work $-\theta'(0)/\sqrt{2}$	Chen and Chen [10] $-\theta'(0)$	Present work $f(\infty)\cdot\sqrt{2}$	Chen and Chen [10] $f(\infty)$
$n = 0.8$	0.423708989	0.4238	1.4223326	1.421
$n = 1.0$	0.443751931	0.4437	1.6169357	1.618
$n = 2.0$	0.490593371	0.4938	2.4017589	2.403

or the surface dimensionless local heat transfer rate $q_w^*(x)$ is

$$q_w^*(x) = \frac{q_w(x)l}{(T_w - T_\infty)k_{ef}} = -Ra_n^{1/2}\theta'(0)\left[\frac{\partial\eta}{\partial y^*}\right]. \tag{29}$$

The local Nusselt number Nu_x can be expressed as

$$Nu_x = \frac{hx}{k_{ef}} = \frac{q_w x}{k_{ef}(T_w - T_\infty)} = -\frac{Ra_n^{1/2}x}{l}\theta'(0)\frac{\partial\eta}{\partial y^*} \tag{30}$$

where h denotes the local heat transfer coefficient and k_{ef} indicates the effective thermal conductivity of the non-Newtonian fluid-saturated porous medium.

The average heat transfer coefficient $\bar{h}$ will be

$$\bar{h} = \frac{1}{l}\int_0^l h\,dx = -\frac{k_{ef}}{l}(\sqrt{Ra_n})\theta'(0)\int_0^1 \frac{\partial\eta}{\partial y^*}dx^* \tag{31}$$

and the average Nusselt number, $\overline{Nu}$, can be expressed as

$$\overline{Nu} = \frac{\bar{h}l}{k_{ef}} = -\theta'(0)\int_0^1 \frac{\partial\eta}{\partial y^*}dx^*. \tag{32}$$

Hence, the overall surface heat transfer rate would be

$$Q^* = \int_0^l q_w(x)[2\pi l]^m W^{(1-m)}\,dx/[l^2 k_{ef}(T_w - T_\infty)] \tag{33}$$

$$= (\sqrt{Ra_n})[2\pi]^m[W/l]^{(1-m)}\theta'(0)\int_0^1 \frac{\partial\eta}{\partial y^*}(r^*)^m\,dx^*$$

where W is the width of the two-dimensional body.

RESULTS AND DISCUSSION

Numerical solution in this study was obtained by using the fourth-order Runge–Kutta scheme and the shooting method. For Case 1, the step-sizes (increments) $\Delta\eta = 0.05$ and $\eta_\infty = 15$ were used. The values of $[-\theta(0)]$ for various values of power index n are shown in Table 1. It can be seen that the agreement is good by comparing with the results reported by Chen and Chen [10]. Figure 2 shows the effects of the power index n on the dimensionless temperature and

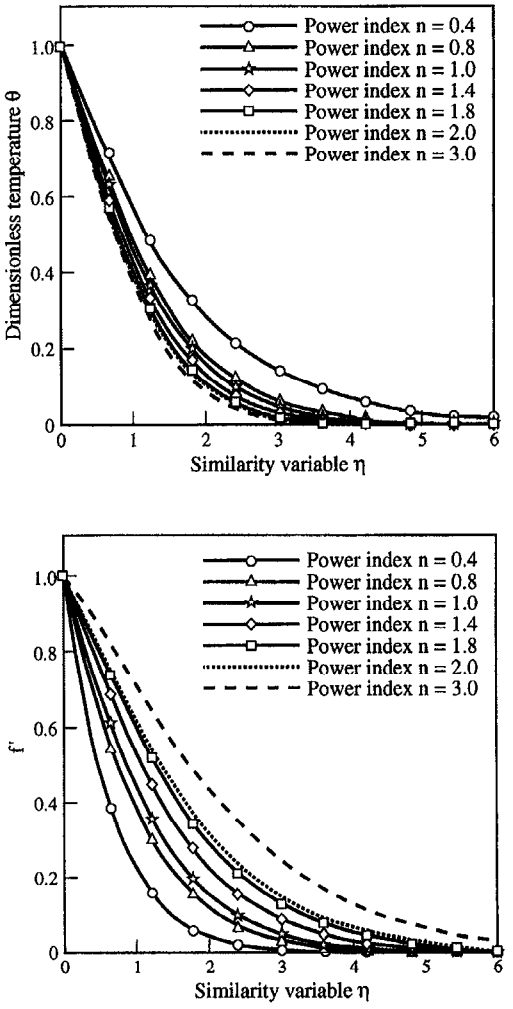

Fig. 2. Dimensionless temperature and velocity profiles vs η for various values of power index n in Case 1.

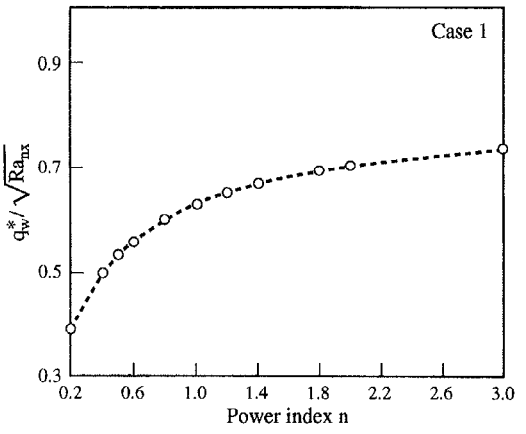

Fig. 3. Various $q_w^*/\sqrt{Ra_n}$ or $[-\theta'(0)]$ vs n in Case.1.

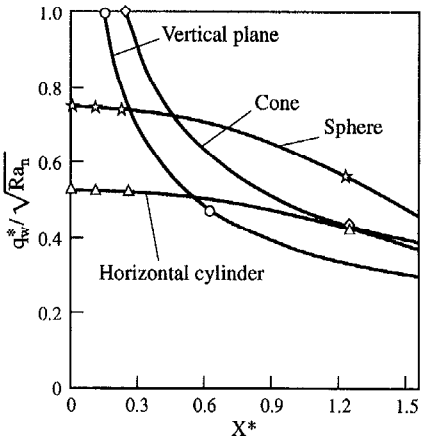

Fig. 4. The local surface heat transfer rate component $q_w^*/\sqrt{Ra_n}$ at the boundary.

velocity distributions. The expressions for momentum and thermal boundary layer thickness can be obtained from equation (18) if the edges of the boundary layers are defined as the points where θ or $[f'(\eta)/f'(0)]$ have a value of 0.01. It is seen from Fig. 2 that the dimensionless thermal boundary layer thickness δ_t increases as n decreases and the dimensionless momentum boundary layer thickness δ_m increases with n. It is found that any two-dimensional or axisymmetric body of arbitrary geometric configuration is possessed of similarity solutions, and equations (29)–(33), respectively, can be rewritten as:

$$q_w^*(x)/\sqrt{Ra_{nx}} = -\theta'(0)/\sqrt{2} \tag{34}$$

where

$$\sqrt{Ra_{nx}} = (\sqrt{Ra_n})(r^*)^m S^{1/n}\left[\int_0^{x^*}(r^*)^{2m}S^{1/n}\,dx^*\right]^{-1/2}$$

$$Nu_x/\sqrt{Ra_{nx}} = -\theta'(0)(x/l)/\sqrt{2} \tag{35}$$

$$\bar{h}/\overline{Ra_n}^{1/2} = -k_{cf}\theta'(0)/[(\sqrt{2})i] \tag{36}$$

$$\overline{Nu}/\overline{Ra_n}^{1/2} = -\theta'(0)/\sqrt{2} \tag{37}$$

$$Q^* = (\sqrt{Ra_n})[2\pi]^m[W/l]^{1-m}[-\theta'(0)] \times \int_0^1 [(r^*)^{2m}S^{1/n}]/\left[(\sqrt{2})\int_0^{x^*}(r^*)^{2m}S^{1/n}\,dx^*\right]dx^* \tag{38}$$

where

$$\overline{Ra_n}^{1/2} = Ra_n^{1/2}\int_0^1 (r^*)^m S^{1/n} \times\left[\int_0^{x^*}(r^*)^{2m}S^{1/n}\,dx^*\right]^{-1/2}dx^*.$$

In Fig. 3, the abscissa variable is the power index n, while the ordinate variable is taken as $q_w^*/\sqrt{Ra_{nx}}$ such that we can easily find that the dimensionless temperature gradient on the wall $[-\theta'(0)]$ increases with n. Figure 4 shows the surface dimensionless local heat transfer rates on a vertical flat plate, a horizontal circular cylinder, a vertical cone with $\phi = \pi/3$, and a sphere computed from equation (30) when $n = 1.0$. It is found from Fig. 4 that the vertical flat plate and cone at $x = 0$ are singular points and there are maximum heat transfer rates on the surfaces of any arbitrary axisymmetric bodies at the lowest point.

The $[-\theta'(0)]$ values are listed in Table 2 for a wide range of power indexes n and yield stress parameters Ω/a for Case 2, for which the step-size $\Delta\eta = 0.1$, and η_∞ being assumed as increasing with Ω/a. The dimensionless temperature profiles $\theta(\eta)$ and the dimensionless velocity distributions $f'(\eta)$ are computed from equations (21) and (27) by the fourth-order Runge–Kutta scheme for $\Omega/a = 0.01$, 0.1, 0.4 and 0.8. The results are presented in Figs. 5–8, respectively, which demonstrate the dimensionless thermal boundary layer thickness δ_t increasing with Ω/a and the dimensionless momentum boundary layer thickness δ_m decreasing with Ω/a. It can be found from Figs. 5–8 that the values of θ approach zero at values of η which increase with the yield stress parameter Ω/a. In addition, the values of $f'(\eta)$ approach zero at appropriate values of η which increase as Ω/a decreases. It should be noted that the profiles of the dimensionless velocity $f'(\eta)$ for $n > 1.0$ are quite different from those for $n \leqslant 1.0$. Equations (29)–(33) are rewritten as the following equations for Case 2:

$$q_w^*(x) = -\theta'(0)(a-\Omega)^{1/2n}\sqrt{Ra_{nx}} \tag{39}$$

where

$$\sqrt{Ra_{nx}} = (\sqrt{Ra_n})(\sqrt{3})^m/[(\sqrt{2})(x/l)^{1/2}] \tag{40}$$

$$Nu_x = -\theta'(0)(a-\Omega)^{1/2n}(x/l)\sqrt{Ra_{nx}}$$

$$\bar{h}^* = -\theta'(0)(a-\Omega)^{1/2n}\overline{Ra_n}^{1/2} \tag{41}$$

$$\overline{Nu} = -\theta'(0)(a-\Omega)^{1/2n}(\sqrt{Ra_n})(\sqrt{3})^m\sqrt{2} \tag{42}$$

Table 2. Values of $[-\theta'(0)]$ in the Case 2 for selected values of power index n (present work: $[-\theta'(0)(1-\Omega/a)^{1/2n}/\sqrt{2}]$)

$-\theta'(0)$	$\Omega/a = 0.8$	$\Omega/a = 0.6$	$\Omega/a = 0.4$	$\Omega/a = 0.1$	$\Omega/a = 0.01$
$n = 0.4$	0.2360206	0.3293941	0.3978876	0.4766793	0.4964553
$n = 0.8$	0.2926623	0.4057788	0.4866598	0.5817668	0.5969870
$n = 1.0$	0.3098622	0.4286398	0.5128838	0.6041183	0.6253583
$n = 1.2$	0.3228418	0.4463470	0.5329725	0.6255285	0.6466230
$n = 1.4$	0.3336272	0.4604560	0.5488637	0.6422950	0.6631720
$n = 2.0$	0.3560082	0.4896445	0.5682714	0.6762185	0.6963369
$n = 3.0$	0.3773161	0.5172694	0.5757589	0.6117710	0.7257282

$-\theta'(0)$	Present $\Omega/a = 0.8$	Wang and Tu [14] $\Omega/a = 0.8$	Present $\Omega/a = 0.6$	Wang and Tu [14] $\Omega/a = 0.6$	Present $\Omega/a = 0.4$	Wang and Tu [14] $\Omega/a = 0.4$
$n = 0.4$	0.046053	0.0699	0.074093	0.0965	0.148571	0.156
$n = 0.8$	0.075683	0.0981	0.161831	0.168	0.250066	0.255
$n = 1.0$	0.097987	0.115	0.1916935	0.196	0.280918	0.282
$n = 1.2$	0.116745	0.130	0.215451	0.218	0.304616	0.305

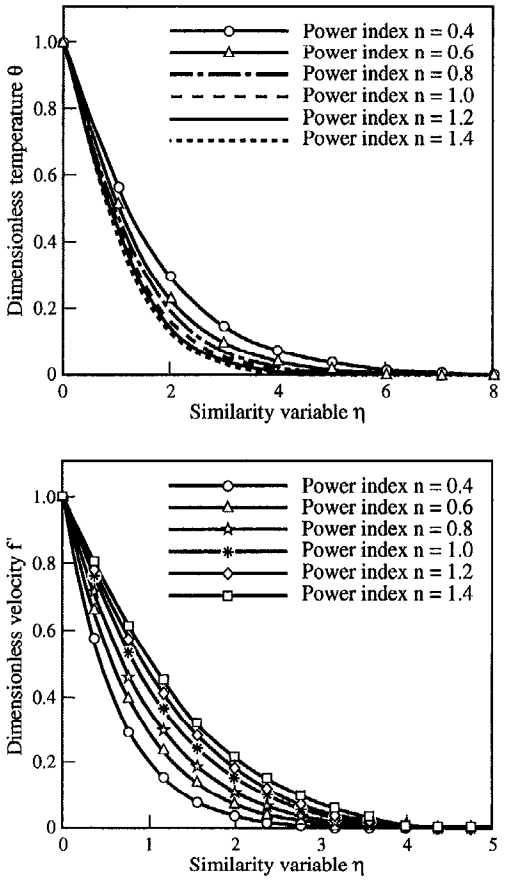

Fig. 5. Dimensionless temperature and velocity profiles vs η for various values of power index n when $\Omega/a = 0.01$ in Case 2.

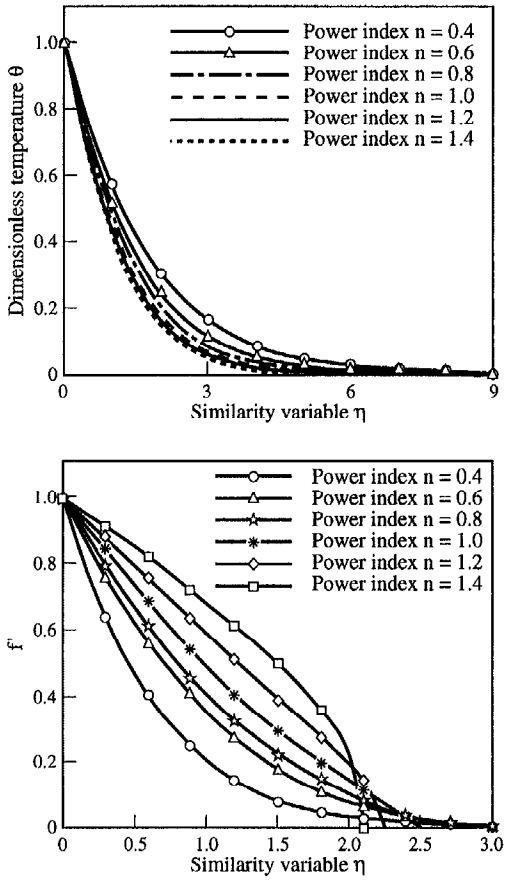

Fig. 6. Dimensionless temperature and velocity profiles vs η for various values of power index n when $\Omega/a = 0.1$ in Case 2.

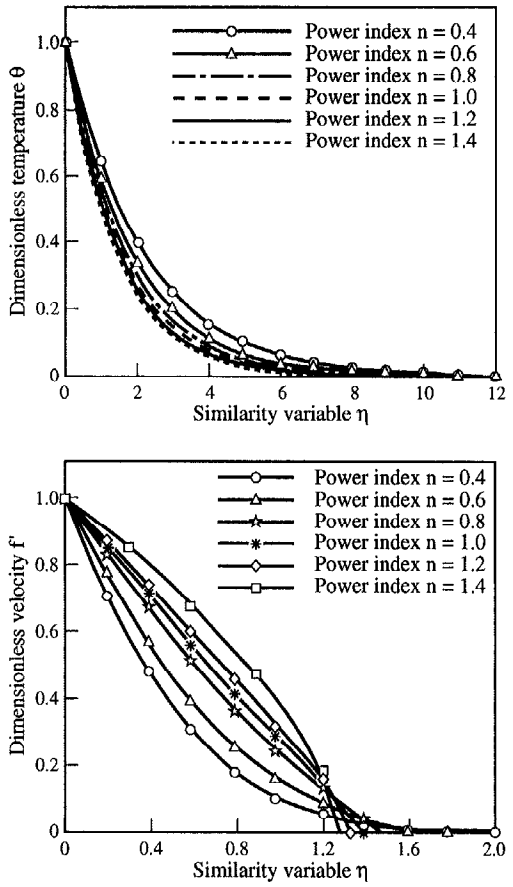

Fig. 7. Dimensionless temperature and velocity profiles vs η for various values of power index n when $\Omega/a = 0.4$ in Case 2.

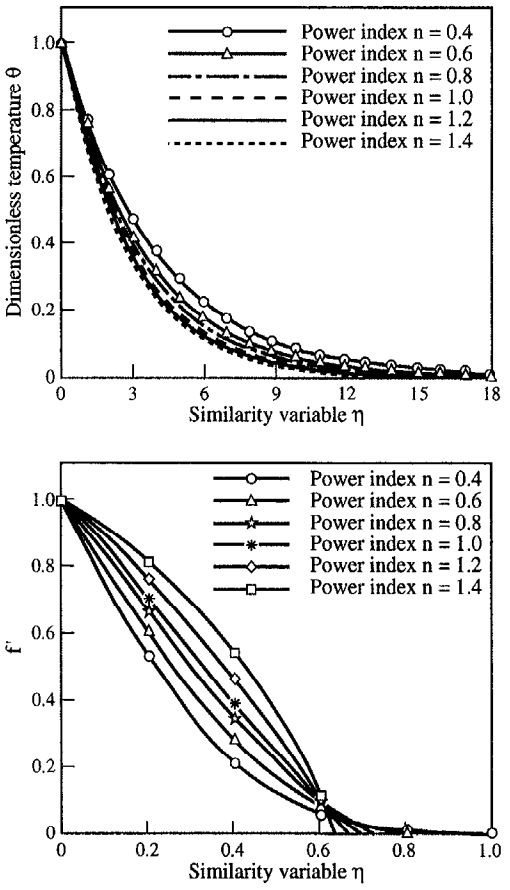

Fig. 8. Dimensionless temperature and velocity profiles vs η for various values of power index n when $\Omega/a = 0.8$ in Case 2.

$$\frac{Q^*}{\sqrt{Ra_n}} = \frac{-\theta'(0)}{l(2m+1)}(a-\Omega)^{1-2n} \times [2\pi l\sqrt{3}(1-aa)]W^{(1-m)}\sqrt{2} \quad (43)$$

where

$$\overline{Ra_n} = (\sqrt{Ra_n})(\sqrt{3})^m(\sqrt{2})(k_{et}/l).$$

The values of $\bar{h}^*/\sqrt{Ra_n}$ increase with the power index n. An open and shut case can be found in Fig. 9 and 10. The value of $\bar{h}^*/\sqrt{Ra_n}$ decreases when the angle ϕ of a cone increases, Ω/a increases or the power index n decreases in Figs. 9 and 10. The local surface heat flux $q_w^*/\sqrt{Ra_n}$ of a increases with the power index n, as shown in Fig. 11. Figure 12 would be valuable to choose the best angle of a cone in order to provide the maximum overall surface heat flux.

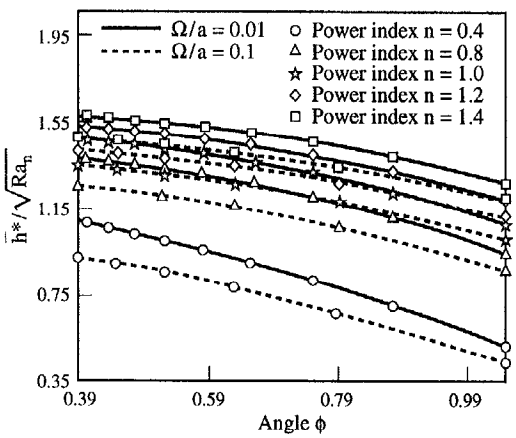

Fig. 9. Values of $\bar{h}^*/\sqrt{Ra_n}$ vs ϕ for various values of n and Ω.

CONCLUDING REMARKS

The present study provides the modified Darcy's law with the Hershel–Bulkley model for solving the external problem of natural convection of a non-Newtonian power-law fluid in the porous media adjacent to the impermeable axisymmetric or two-dimensional bodies, where the surface temperature is constant. Similarity solutions of two cases were obtained by using the fourth-order Runge–Kutta method. It was

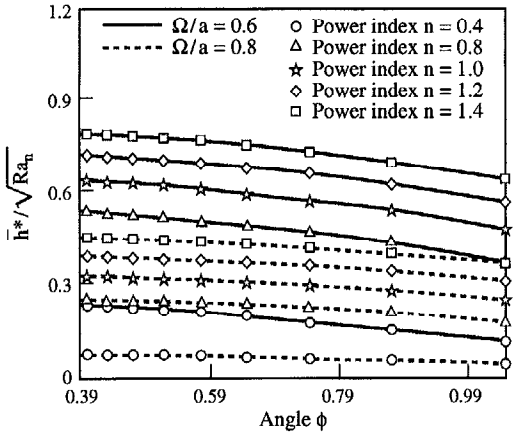

Fig. 10. Values of $\bar{h}^*/\sqrt{Ra_n}$ vs ϕ for various values of n and Ω.

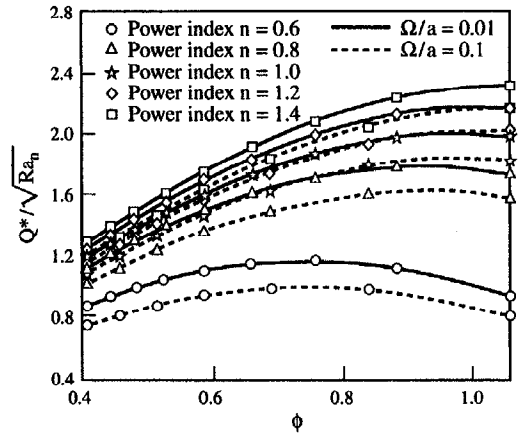

Fig. 12. The overall surface heat transfer rate $Q^*/\sqrt{Ra_n}$ vs ϕ for various values of n and of Ω/a.

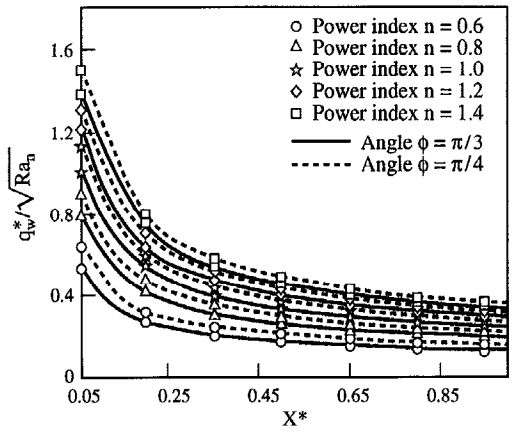

Fig. 11. The local surface heat transfer rate $q_w^*/\sqrt{Ra_n}$ of a cone for various values of n and ϕ.

found that the temperature profiles and the velocity profiles are strongly dependent on the high yield stress parameters.

REFERENCES

1. P. Cheng and I.-D. Chang, Buoyancy induced flows in a saturated porous medium adjacent to impermeable horizontal surfaces, *Int. J. Heat Mass Transfer* **19,** 1267–1272 (1976).
2. J. H. Merkin, Free convection boundary layers on axisymmetric and two-dimensional bodies of arbitrary shape in a saturated porous medium, *Int. J. Heat Mass Transfer* **22,** 1461–1462 (1979).
3. T. Y. Na and I. Pop, Free convection flow past a vertical plate embedded in a saturated porous medium, *Int. J. Engng Sci.* **21,** 517–526 (1983).
4. A. Nakayama and H. Koyama, Free convection heat transfer over a non-isothermal body of arbitrary shape embedded in a fluid-saturated porous medium, *J. Heat Transfer* **109,** 125–130 (1987).
5. R. H. Christopher and S. Middleman, Power-law flow through a packed tube, *I&EC Fundam.* **4,** 422–426 (1965).
6. A. Acrivos, M. J. Shan and E. E. Petersen, Momentum and heat transfer in laminar boundary layer flow of non-Newtonian fluids past external surfaces, *A.I.Ch.E. Jl* **6,** 312–317 (1960).
7. A. Acrivos, A theoretical analysis of laminar natural convection heat transfer to non-Newtonian fluids, *A.I.Ch.E. Jl* **6,** 584–590 (1960).
8. T. AL-Fariss and K. L. Pinder, Flow through porous media of a shear-thinning liquid with yield stress, *Can. J. Chem. Engng* **65,** 391–404 (1987).
9. C. K. Chen and H. T. Chen, Natural convection of non-Newtonian fluids about a horizontal surface in a porous medium, *Energy Resources Technol. J.* **109,** 119–123 (1987).
10. C. K. Chen and H. T. Chen, Natural convection of a non-Newtonian fluid about a horizontal cylinder and a sphere in a porous medium, *Int. Commun. Heat Mass Transfer* **15,** 605–614 (1988).
11. C. K. Chen and H. T. Chen, Natural convection of non-Newtonian fluids along a vertical plate embedded in a porous medium, *J. Heat Transfer, ASME* **110,** 257–260 (1988).
12. H. Pascal, Rheological behaviour effect of non-Newtonian fluids on steady and unsteady flow through a porous medium, *Int. J. Numer. Analytical Meth. Geomech.* **7,** 289–303 (1983).
13. H. Pascal, Nonsteady flow of non-Newtonian fluids through a porous medium, *Int. J. Engng Sci.* **21,** 199 210 (1983).
14. Wang Chaoyang and Tu Chuanjing, Boundary-layer flow and heat transfer of non-Newtonian fluid in porous media, *Int. J. Heat Fluid Flow* **10,** 160–165 (1989).
15. R. B. Bird, *Transport Phenomena* (1960).